Report No. K-TRAN: KSU-98-2
FINAL REPORT

PILOT INSTRUMENTATION OF A SUPERPAVE TEST SECTION AT THE KANSAS ACCELERATED TESTING LABORATORY

Zhong Wu
Mustaque Hossain, Ph.D., P. E.

Kansas State University
Manhattan, Kansas

APRIL 2003

K-TRAN

A COOPERATIVE TRANSPORTATION RESEARCH PROGRAM BETWEEN:
KANSAS DEPARTMENT OF TRANSPORTATION
KANSAS STATE UNIVERSITY
THE UNIVERSITY OF KANSAS

1 Report No. KTRAN: KSU-98-2	2 Government Accession No.	3 Recipient Catalog No.
4 Title and Subtitle PILOT INSTRUMENTATION OF A SUPERPAVE TEST SECTION AT THE KANSAS ACCELERATED TESTING LABORATORY		5 Report Date April 2003 6 Performing Organization Code
7 Author(s) Zhong Wu and Mustaque Hossain, Ph.D., P.E., Kansas State University		8 Performing Organization Report No.
9 Performing Organization Name and Address Kansas State University Department of Civil Engineering Manhattan, Kansas 66506		10 Work Unit No. (TRAIS) 11 Contract or Grant No. C1107
12 Sponsoring Agency Name and Address Kansas Department of Transportation Bureau of Materials and Research, Research Unit 2300 Southwest Van Buren Street Topeka, Kansas 66611-1195		13 Type of Report and Period Covered Final Report August 1998 – November 2000 14 Sponsoring Agency Code RE-0126-01

15 Supplementary Notes
For more information write to address in block 9.

16 Abstract

Two Superpave test sections were constructed at the Kansas Accelerated Testing Laboratory (K-ATL) with 12.5 mm (**2** in) nominal maximum size Superpave mixture (SM-2A) with varying percentages (15 and 30 percent) of river sand. A 150 kN (34 kip) tandem axle with dual wheels was used for 10,000 repetitions. Next the sections were loaded by three different tandem axle loads and three single axles for more than 30 repetitions in each configuration to estimate the relative pavement damage in the SM-2A layer due to different axle loads and configurations. All load application was done at a temperature of approximately 38^{o} C (98^{o} F) at the middle of the SM-2A layer. The test sections were instrumented at three locations on each test section with (i) transverse strain gages at the bottom of the SM-2A layer, (ii) pressure cells on the top of the subgrade, and (iii) temperature gages in the aggregate base, subgrade and SM-2A layers (mid-depth and bottom). Data was collected during load applications by the K-ATL tandem axle and a Falling Weight Deflectometer (FWD). After 80,000 applications of the 150 kN (34 kip) tandem axle loading, severe rutting was observed on both test sections with no visible cracking, and the testing was terminated.

The theoretical pavement responses were also calculated with a multi-layer elastic analysis program, ELSYM5 and compared to the test results. The measured vertical stresses on the top of the subgrade and tensile strains at the bottom of the SM-2A layer due to FWD loads are generally very close to those calculated by ELSYM5. However, measured tensile strains and vertical stresses on both sections were higher than those calculated by ELSYM5. In general, the measured tensile strains under the K-ATL wheel loads were found to increase with increasing number of wheel load repetitions, but the measured vertical stresses remained relatively constant.

Fatigue tests were conducted on the beams fabricated from the loose SM-2A (15) mixtures sampled during construction. Fatigue and rutting damage analyses were also conducted on a set of test beams sawed from that section. The rutting and fatigue results were consistent with observed and predicted damage. The AASHTO load equivalency factors were found to be much higher than those calculated in this study. Finally, based on the measured pavement temperature data and the longitudinal profile data (dipstick measurement), a temperature variation along the depth of Superpave pavements and pavement deterioration based on International Roughness Index values were analyzed and reported. Several recommendations based on this study have also been made.

16 Key Words	17 Distribution Statement
Crack, Falling Weight Deflectometer, Fatigue Test, FWD, Mixture, Superpave, Sand, Tandem Axle, Tensile Strain	No restrictions. This document is available to the public through the National Technical Information Service, Springfield, Virginia 22161

18 Security Classification (of this report)	19 Security Classification (of this page)	20 No. of pages	21 Price
Unclassified	Unclassified	66	

Form DOT F 1700.7 (8-72)

PILOT INSTRUMENTATION OF A SUPERPAVE TEST SECTION AT THE KANSAS ACCELERATED TESTING LABORATORY

Final Report

Prepared by

Zhong Wu
Kansas State University

and

Mustaque Hossain, Ph.D., P.E.
Kansas State University

A Report on Research Sponsored By

THE KANSAS DEPARTMENT OF TRANSPORTATION
TOPEKA, KANSAS

KANSAS STATE UNIVERSITY
MANHATTAN, KANSAS

April 2003

PREFACE

The Kansas Department of Transportation's (KDOT) Kansas Transportation Research and New-Developments (K-TRAN) Research Program funded this research project. It is an ongoing, cooperative and comprehensive research program addressing transportation needs of the state of Kansas utilizing academic and research resources from KDOT, Kansas State University and the University of Kansas. Transportation professionals in KDOT and the universitiesjointly develop the projects included in the research program.

NOTICE

The authors and the state of Kansas do not endorse products or manufacturers. Trade and manufacturers names appear herein solely because they are considered essential to the object of this report.

This information is available in alternative accessible formats. To obtain an alternative format, contact the Office of Transportation Information, Kansas Department of Transportation, 915 SW Harrison Street, Room 754, Topeka, Kansas 66612-1568 or phone (785) 296-3585 (Voice) (TDD).

DISCLAIMER

The contents of this report reflect the views of the authors who are responsible for the facts and accuracy of the data presented herein. The contents do not necessarily reflect the views or the policies of the state of Kansas. This report does not constitute a standard, specification or regulation.

ABSTRACT

This report describes the instrumentation and test results from two 2.4 m (8 ft) by 6.1 m (20 ft) Superpave test sections at the Kansas Accelerated Testing Laboratory (K-ATL). Both sections were constructed with 12.5 mm (1/2 in) nominal maximum size Superpave mixture (SM-2A) with varying percentages (15 to 30 percent) of river sand. A 150 kN (34 kip) tandem axle with dual wheels and 620 kPa (90 psi) tire pressure was used for loading. After 10,000 repetitions, the sections were loaded by 160 kN (36 kip), 150 kN (34 kip) and 144 kN (32.5 kip) tandem axles and 98 kN (22 kip), 90 kN (20 kip), and 80 kN (18 kip) single axles for more than 30 repetitions in each configuration. This was done to estimate the relative pavement damage in the SM-2A layer due to different axle loads and configurations. All load application was done at about 38° C (98° F) temperature at the middle of the SM-2A layer. The test sections were instrumented at three locations on each test section with:

(i) transverse strain gages at the bottom of the SM-2A layer,

(ii) pressure cells on the top of the subgrade, and

(iii) temperature gages in the aggregate base, subgrade and SM-2A layers (mid-depth and bottom).

Data was collected using an interface developed with LabView during load applications by the K-ATL tandem axle and a Falling Weight Deflectomter (FWD). After 80,000 applications of the 150-kN (34-kip) tandem axle loading, severe rutting was observed on both test sections with no visible cracking, and the testing was terminated.

The theoretical pavement responses were also calculated from a multi-layer elastic analysis program, ELSYM5. The results show that measured vertical stresses on the top of the subgrade and tensile strains at the bottom of the **SM-2A** layer due to FWD loads are generally very close to those calculated by **ELSYMS.** Under the **K-ATL** wheel loads, the **SM-2A** mixture with 15% river sand, **SM-2A** (15), had higher calculated and measured tensile strains at the bottom of the **SM-2A** layer and the vertical stresses on the top **of** the subgrade than the **SM-2A** mixture with 30% river sand, **SM-2A** (30). This is true for both the average measured value and individual gage locations (stations). However, measured tensile strains and vertical stresses on both sections were higher than those calculated by ELSYM5. In general, the measured tensile strains were found to increase with increasing number of wheel load repetitions, and the measured vertical stresses remained relatively constant.

Fatigue tests were conducted on the beams fabricated in the laboratory from the loose **SM-2A** (15) mixtures sampled during construction. **A** second set of test beams were also sawed from that section. Fatigue and rutting damage analyses were then conducted. The results indicated very little fatigue damage on these sections which was consistent with the visual observations at the surface and in a trench cut through the test sections. Good consistency between the predicted and actual rut depths was observed when the initial densification **of** the Superpave mixtures on the test sections was considered in the analysis process. For **SM-2A** (30), most of the rutting happened due to shear flow of the Superpave mixture. However, for **SM-2A** (15), rutting happened mainly due to consolidation of the Superpave mixture and/or the base layer since no significant flow of the Superpave mixture was evident. The AASHTO load equivalency factors were found to be much higher than those calculated in this study.

Finally, based on the measured pavement temperature data and the longitudinal profile

data (dipstick measurement), a temperature variation along the depth of Superpave pavements and pavement deterioration based on International Roughness Index values were analyzed and reported. Several recommendations based on this study have **also** been made.

ACKNOWLEDGMENTS

The authors gratefully acknowledge the financial support by the Kansas Department of Transportation (KDOT) under the K-TRAN program. Cooperation of Mr. Paul Lewis, Mr. Don Bruns and Ms. Swetha Chitrapu, all of Kansas State University; Mr. Andy Gisi, Mr. Albert Oyerly, Mr. Glenn Fager and the Falling Weight Deflectometer (FWD) crew, all of KDOT, in this study is also acknowledged. The transverse profile data used in this study was collected in a concurrent study at K-ATL (KS-2) funded by the Mid-West States Accelerated Testing Pooled Fund Program. Dr. Hani Melhem was the Principal Investigator of that project.

TABLE OF CONTENTS

LIST OF TABLES

LIST OF FIGURES

CHAPTER 1

INTRODUCTION

1.1 Introduction

A critical problem for the pavement engineer is the design of heavy-duty pavements where traffic load differs significantly in weight, number, and/or configuration from previous experience (McGennis et al. 1994). The traditional method of establishing a satisfactory design is to build an experimental pavement section of pavement based on a hypothesis, observe the behavior, and then quantify the performance of the pavement under in-service traffic. However, this approach may not provide sufficient or timely guidance. Even where such an experiment can be conducted on a major route, it is still possible that the rate of growth of traffic load on the in-service pavements will exceed the loading accumulated by the experimental pavement so that no reliable predictive basis can be established. This problem can occur when highway pavements experience unanticipated traffic growth as has been manifested on 1-435 in Johnson County, Kansas. The Daily Vehicles Miles Traveled (DVMT) in Kansas has increased 14 percent between 1993 and 1997 as shown in Figure 1. Truck travel (Truck DVMT) has increased 32.5 percent between 1993 and 1997. Truck axle weights also have shown significant growths on nearly all major US routes and all Interstate routes in Kansas. The pavement engineers also need to evaluate the potential of new materials or mixture design, such as the Superpave mixture design system, in a timely manner to take into account the advancement in practice. A number of problems are associated with the experimental test sections performed under traffic conditions:

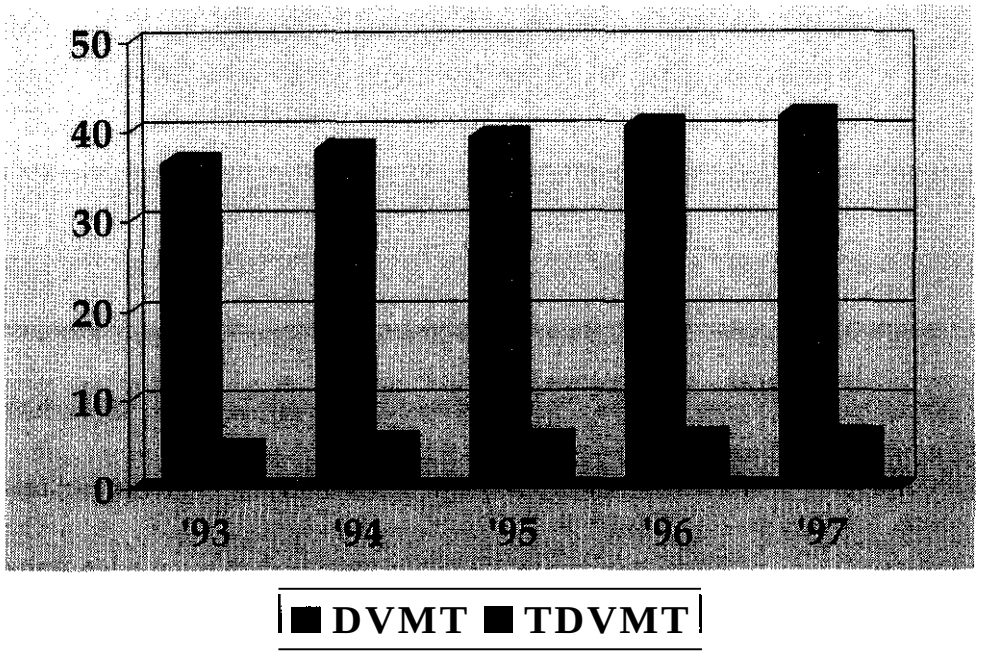

FIGURE 1: Trends of Daily Vehicle Miles Traveled (DVMT) and Truck Daily Vehicle Miles Traveled (TDVMT) in Kansas, in Millions

(i) Insufficient time exists to collect and analyze performance data;

(ii) The consequence of unsatisfactory performance of a new material, a different pavement configuration, or the impact of increased loading results in a severe loss of serviceability; and

(iii) The variability of the parameters affecting behavior and performance, such as frequency of loading, material properties, and climate (Metcalf 1998).

Under these circumstances a methodology, like the accelerated load testing, is needed to allow exploration of new pavement mixtures or cross section design with controlled traffic loading parameters that can accumulate damage faster than the anticipated growth of traffic or changes in vehicle technology. Ideally, the method also has to control non-traffic load factors, such as material variability and

environmental variation, to reduce the number of variables in an experiment (Metcalf 1998).

1.2 Problem Statement

Kansas Department of Transportation (KDOT) is considering full implementation **of** the Superpave mixture design by year 2001. Since majority of the pavements in Kansas carry lower traffic volumes, it is anticipated that the Superpave volumetric mix design will be the predominant procedure to be used in the state. However, there is a need for evaluating a pavement structure incorporating Superpave mixture for the critical stress/strain since no performance testing is currently being conducted on the volumetric mixtures. There is also a need for developing relationships between the critical stress/strain and pavement performance in terms of fatigue cracking and rutting, if any mechanistic design is to be satisfied. Therefore, this project was initiated to address the issue of Superpave mixtures with natural (river) sand in "Accelerated Pavement Testing" (APT) at the Kansas Accelerated Testing Laboratory (K-ATL) at Kansas State University.

1.3 Research Objectives

The objective of this study was to instrument two test sections of Superpave mixtures with varying percentage of river sand to measure the following mechanistic parameters for pavement performance evaluation:

(i) tensile strain at the bottom of the asphalt concrete layer; and

(ii) vertical compressive stress on the top of the subgrade.

Instrumentation was also done to measure pavement temperature at four depth locations in each section. The secondary objective of this study was to tie the mechanistic responses with the pavement performance in terms of fatigue damage, rutting and/or serviceability, and Superpave mixture composition.

1.4 Organization of Report

Chapter 1 discusses the problem statement and the objectives of this study. Chapter 2 describes the instrumentation of two Superpave test sections at K-ATL. Chapter 3 discusses the laboratory fatigue tests done at Kansas State University (KSU) and interpretation of the results. Chapter 4 addresses the differences between the measured and calculated pavement responses under the Falling Weight Deflectometer (FWD) loading and the wheel loading. Chapter 5 contains the analysis of fatigue damage and permanent damage (rutting) in terms of damage ratio. Chapter 6 further analyzes the rutting damage based on the method of deformed area. Chapter 7 reports the measured pavement temperature distribution and evaluates the roughness development based on the International Roughness Index (IRI) values. Chapter 8 describes the relative pavement damage from a comparison of the computed equivalent axle load factor (EALF) ratios from the American Association of State Highway and Transportation Officials (AASHTO) and the laboratory fatigue equations developed in this study. Chapter 9 presents the conclusions of this study.

CHAPTER 2

INSTRUMENTATION OF TEST SECTIONS

2.1 Kansas Accelerated Testing Laboratory (K-ATL)

The K-ATL is an indoor facility with about 651 m^2 (7,000 ft^2) floor space for accelerated testing of pavement sections. The pavements are constructed in two 1.83 m (6 ft) deep test pits of varying width and 6.1 m (20 ft) length. The load frame has two main girders and columns made of W30×99 rolled beams with 12.8 m (42 ft) center-to-center span. A carriage is suspended from the girders. This allows the carriage to be removed from the test slab before it goes back in the opposite direction for unidirectional testing. At the end of a pass along a test section, an energy absorption/release system (springs) helps transform the kinetic energy of the carriage into potential energy in the springs, and then back to kinetic energy, reversing the direction of the carriage. The wheel load assembly consists of a tandem axle with an air bag suspension system. Loading of the axle assembly is accomplished with air pressure with the system being loaded on one or both axles as desired. The system applies loads in both directions as the axle assembly moves back and forth using a drive belt system. However, the air pressure can be removed from the system when the assembly is moving backward if unidirectional traffic on a test section needs to be simulated. The speed gradient used in K-ATL is an acceleration to reach a steady-state speed of 8 km/h (5 mph) for a minimum distance of 4.3 m (14 ft), and then, a deceleration. The assembly takes approximately 7.5 seconds to complete its travel distance for the 6.1 m (20 ft) test section in one direction for a cycle (Vijaynath et al 1999).

In this study, a tandem axle with dual wheels was used for loading. The load magnitude was 150 kN (34 kip) with 620 kPa (90 psi) tire pressure. For the given section, based on the AASHTO

Design Guide, this resulted in approximately 1.08 80 kN (18-kip) Equivalent Single Axles Loads (ESAL's) per repetition of the K-ATL tandem axle assembly.

2.2 Test Section Construction

Two 2.4 m (8 ft) wide and 6.1 m (20 ft) long test sections were constructed with a 12.5 mm ½ in) nominal maximum size Superpave mixture. The combined aggregate gradation *(dry)* of this mixture, designated as SM-2A in Kansas, passes above the restricted zone. Figure 2 shows the outline and cross-sections of the test sections. Figure 3 is the gradation curve for aggregates on both test sections. The mix used on the north section, SM-2A (30), consists of 25 percent Martin-Marietta crushed limestone, 5 percent Martin-Marietta crushed limestone screening, 28 percent Bingham-Cherokee chat, 10 percent manufactured sand, 2 percent dust (baghouse fines) and 30 percent Kansas river sand. The mix on the south section, SM-2A (15), consists of 22 percent Martin-Marietta crushed limestone, 8 percent Martin-Marietta crushed limestone screening, 43 percent Bingham-Cherokee chat, 10 percent manufactured sand, 2 percent dust (baghouse fines) and 15 percent Kansas River sand. The significant difference between these two mixtures is the proportion of river sand. The 30 percent river sand in the mix on the north section has been replaced partially by chat in the mix on the south section. This mixture was used in an overlay on a heavily trafficked concrete Interstate route (1-70) in Kansas. The sand equivalent values for both aggregate blends were similar. The mixture with 15 percent river sand had slightly higher uncompacted void content as shown in Table 1.

Table 1 also compares the design and as-built volumetric and other properties of the Superpave mixtures. Both pavement sections were built at the same time with an automated paver by diverting trucks from the actual overlay project on I-70. At least 100 tons of mixture was produced before building the test sections at the K-ATL. Both mixes met the required Superpave criteria for a 12.5 mm

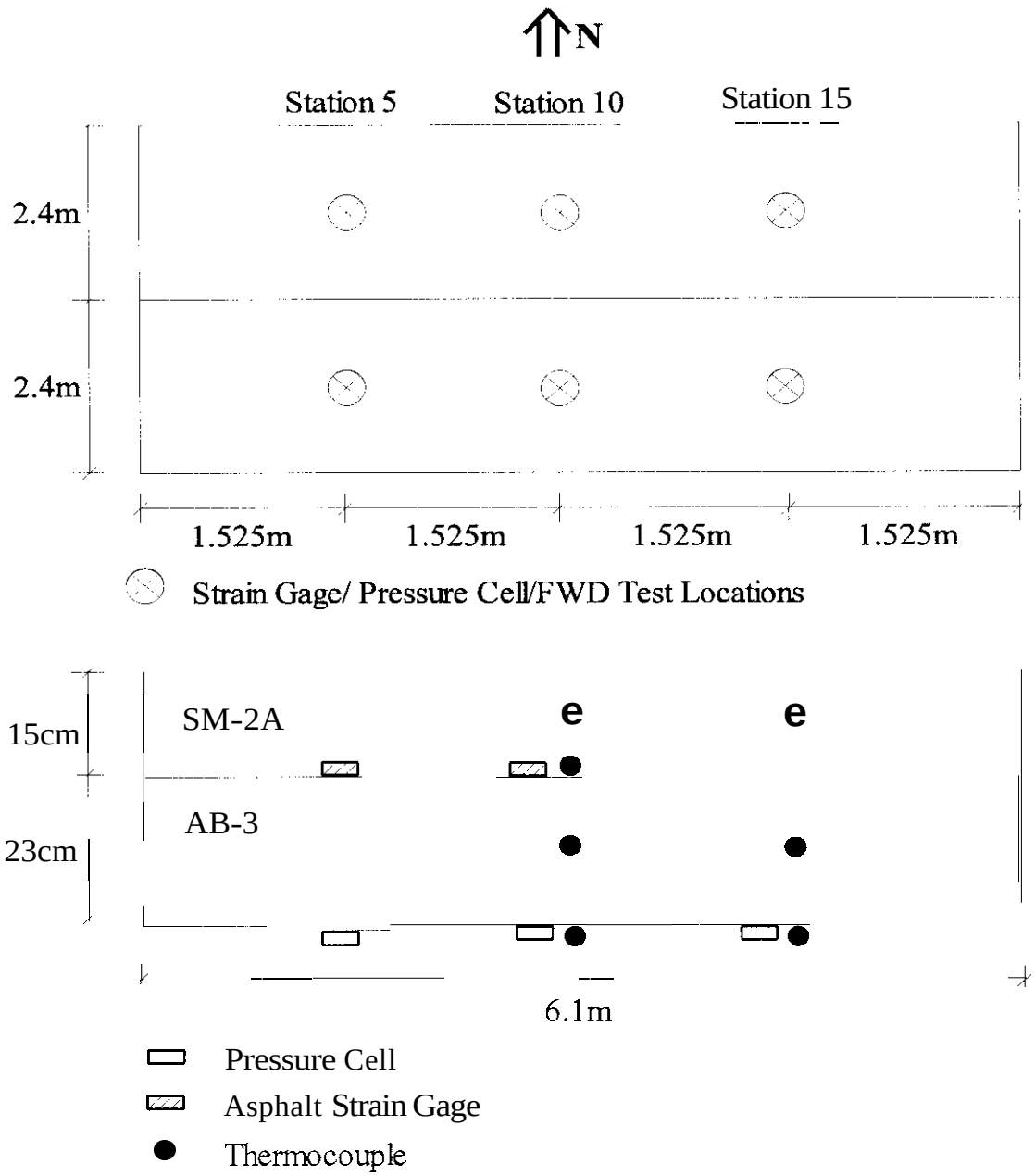

FIGURE 2: Test Section Lavout

(½ in) nominal maximum size Superpave mixture. However, the air voids at N_{des} was 5.6 percent for the north section mixture **(30** percent river sand) compared to **4.4**percent for the south section mixture (15 percent river sand). Excellent compaction (95 percent of G_{mm} or higher) was achieved on both

sections. This quality **of** compaction would qualify the contractor to approximately **4.04** percent bonus according to the KDOT's special provisions for Quality Control/Qaulity Assurance (QC/QA) **of** Superpave Bituminous Pavement Construction.

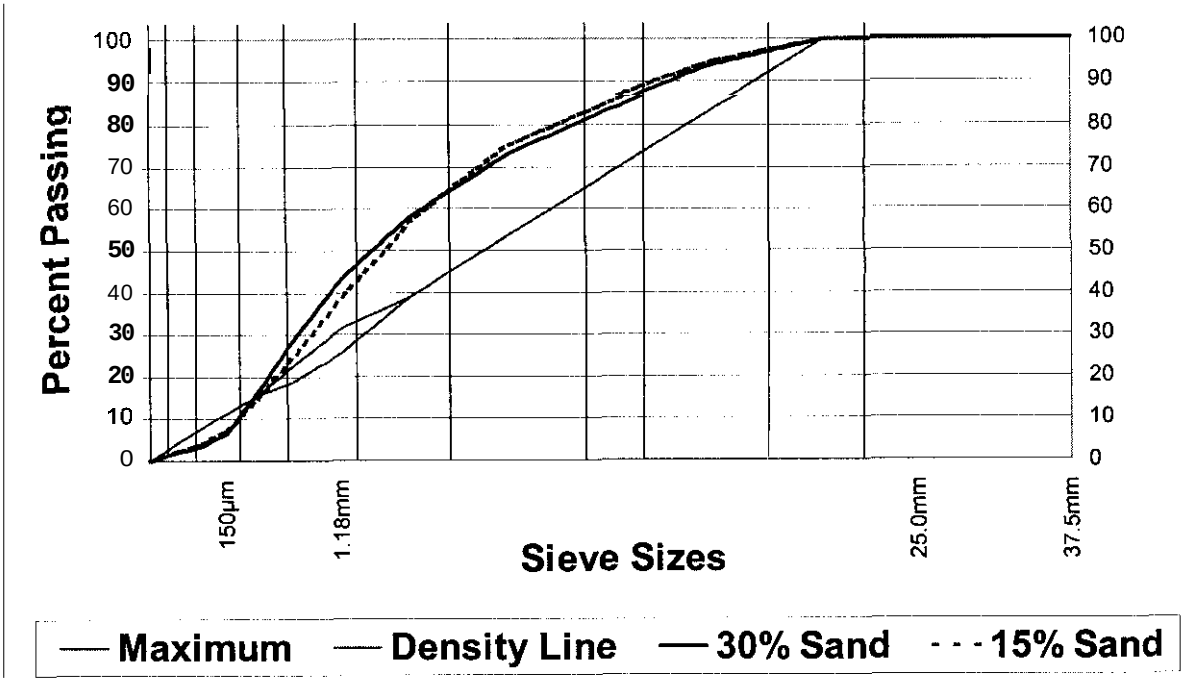

FIGURE 3: Gradation Curves for Superpave Mixtures

TABLE 1: Prouerties of the Superpave Mixtures (N_{design} = 76)

Mixture/Aggregate Blend Property	Required/ Criteria	North Lane *(SM-2A with 30% River Sand)*		South Lane *(SM-2A with 15% River Sand)*	
		Design	As-Built	Design	As-Built
Asphalt Content (%)	-	5.5	6.1	6.7	7.1
Air Voids (%) at N_{des}	4.0	4.0	5.6	4.0	4.4
VMA (%)	14.0 min.	14.1	16.8	16.0	16.2
VFA (%)	65-78	72	66.8	75	72.7
Dust-Binder Ratio	0.6 - 1.2	0.85	0.8	0.90	1.1
Tensile Strength Ratio (TSR)	80% min.	96.1		76.6	-
%Gmm at N_{ini}	89% max.	89.8	88.6	88.0	87.8
%Gmm at N_{max}	98% max.	97.0	95.3	97.3	96.1
Sand Equivalent	40	82	-	80	-
Uncompacted Voids (%)	40	40.7	-	42.9	-
In-Pace Densitv (%G_{mm})[a]	-	94.9		95.5	

[a] Average of three locations.

As shown in Figure 2, a typical section had a 150 mm *(6* in) Superpave mix layer over a 228 mm (9 in) aggregate base (KDOT **AB-3)** and 1.45 m (57 in) soil subgrade. The pavement was underlain by 280 mm (11 in) of pea gravel to facilitate drainage and 228 mm (9 in) of reinforced concrete slab so that no seepage of ground water would be possible.

The subgrade consisted of a typical silty soil (AASHTO A-4) from a pit recently used for a number of road construction projects. The soil had a liquid limit of 28 percent and a plasticity index of 9

percent. Approximately 84 percent of the soil passed a 0.075 mm (No. 200) sieve. The Standard Proctor test showed a maximum *dry* density (MDD) of 1826 kg/m^3 (114 pcf) with 14 percent optimum moisture content (OMC). The soil was placed in the pit in 10 lifts of approximately 150 mm (6 in) each and compacted to 90 percent of the laboratory MDD with a baby sheeps-foot roller. The density obtained was monitored with a nuclear gage. The top 0.46 m (18 in) of the subgrade was compacted to 95 percent of MDD.

The granular base was mostly 19 mm (3/4 in) nominal maximum size crushed limestone (AB-3) with approximately 15 percent passing a No. 200 sieve. This material was placed in loose lift thickness of 150 mm (6 in) and specified to be compacted to 95 percent of the MDD of 2323 kg/m^3 (145 pcf). The optimum moisture content of the AB-3 material was approximately 10 percent (Vijaynath et al 1999).

2.3 Instrumentation

The test sections were instrumented at three locations as shown in Figure 2. Typically, three Dynatest PAST-2AC strain gages were installed at the bottom of the asphalt concrete layer on both sections. On the north section, two strain gages (Dynatest PAST-2AC) were also installed at the mid-depth or interface of two asphalt lifts. Thus, a total of eight asphalt strain gages were installed. Three Geokon 3500 soil pressure cells were installed at the top of the subgrade on each section. At each location, four thermocouples were installed: one at the middle of the asphalt concrete layer, one at the bottom of the asphalt concrete layer, one at the middle of the aggregate base and one at the top of the subgrade. The total number of thermocouples installed was 24.

2.3.1 Dynatest PAST-2AC Strain Gape

The Dynatest PAST-2AC strain gages have been developed based on the experiences of

pavement tests under the Danish Road Testing Machine and at the OECD NARDO experiment in Italy (OECD 1991). The gages designated as "Transverse Embedment Strain Gage (TE)" by MnRoad Research Project in Minnesota have been installed at numerous locations on the MnRoad test sections (Baker and Buth 1994). The type of embedment strain gauge used consists of electrical resistance strain gauges embedded within a strip of lass-fiber reinforced epoxy, with transverse steel anchors at each end of the strip, to form an H-shape. Horizontal strains (in the longitudinal direction) in asphalt concrete are usually measured to collect data related to the current failure criteria used in the mechanistic-empirical pavement design procedures. Figure **4** shows the Dynatest PAST-2AC strain gages and the direction in which they were placed on the test pavements. The data from these gages also provide the means for comparing the in-situ results to those of analytical models.

2.3.2 Dynamic Soil Pressure Cell

The dynamic pressure cells used in this study have been selected based on the experience of MnRoad researchers (Baker and Buth 1994). The MnRoad project has 106 Geokon 3500 Dynamic Soil Pressure Cells with Ashkroft K1 Transducers. Six vertical pressure cell sensors were used in this study, as shown in the Figure 2, to measure vertical stresses at the top of the subgrade layer. These sensors are large diameter soil stress cells consisting **of** two circular steel plates welded together around their rims to create a cell approximately 150 mm (6 in) thick. The space between the plates is liquid-filled. A steel tube connects the liquid to an electrical pressure transducer several centimeters away from the cell. The pressure transducer responds to changes in total stress applied to the material (soil) in which the cell is embedded. Figure 5 shows the Geokon 3500 Dynamic Soil Pressure Cells and the direction in which they were placed on the test pavements.

2.3.3 Thermocouples

The thermocouples used in this project were fabricated in this project. Seventy six meters (250-ft) of Omega thermocouple extension wires (SS-T-20-200) were used in fabrication. The thermocouples were able to measure temperature as high as **169** °C (320 °F). The surface temperature measurement during response monitoring was accomplished by a RayTeK infrared sensor.

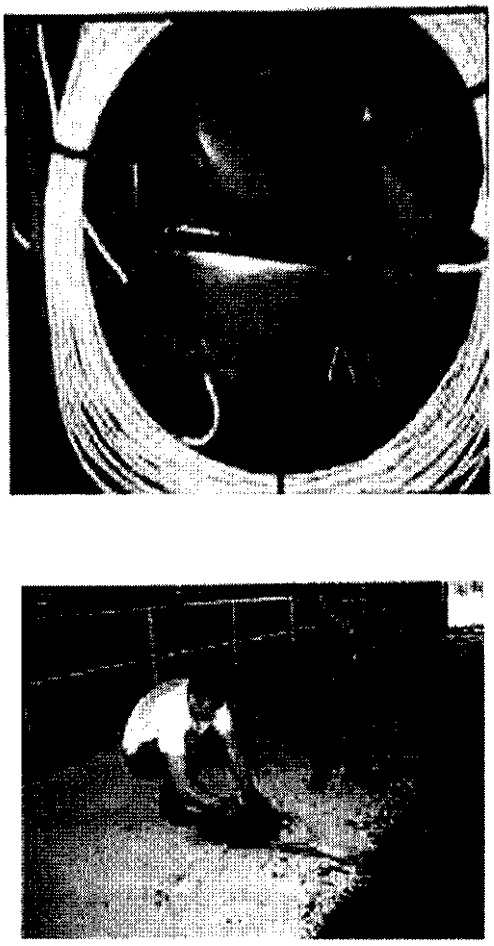

FIGURE 4: Dynatest PAST-2AC Strain Gage and Placement

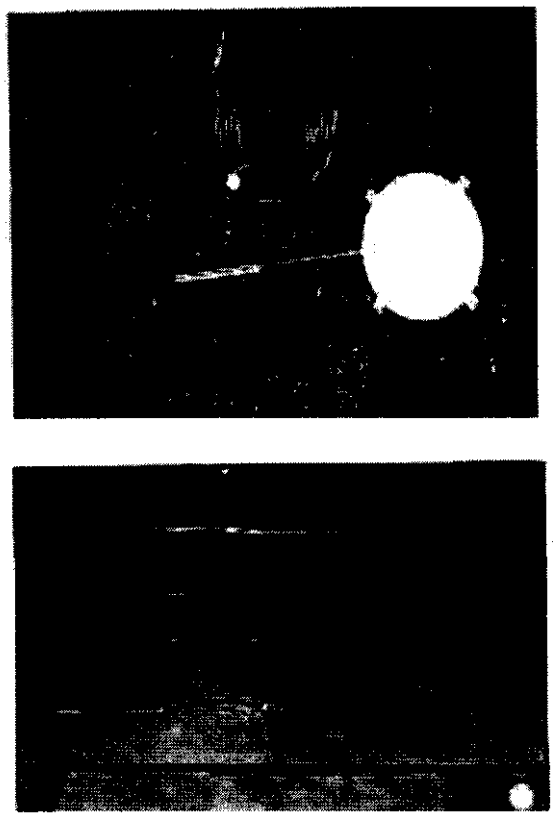

FIGURE 5: Geokon 3500 Dynamic Soil Pressure Cell and Placement

2.3.4 Data Acquisition

This section describes the hardware and software configurations for real-time strain and pressure data acquisition. Most of the hardware used for data acquisition and signal conditioning were manufactured by National Instruments. The software used for acquiring and logging the data were developed using commercial visual application development platform called LabVIEW.

2.3.5 Strain Data Acquisition

A schematic of the strain data acquisition setup is shown in the Figure ***6***. The lead wires from a Dynatest PAST-2AC strain gage were connected to the SCXI-1322 terminal block which, in turn, was connected to the SCXI-1122 signal conditioning module. The SCXI-1122 module provides the

excitation voltage to the strain gage, and a schematic of this bridge configuration is shown in the Figure 7. A dummy resistor with a resistance equal to the strain gage resistance was used to complete the bridge.

The SCXI-1122 signal conditioning module was mounted on a SCXI-1000 chassis. The data acquisition board (AT-MI0 16E-2) was connected to the signal conditioning module through a shielded cable. The data acquisition board was plugged in to an ISA slot of the mother board of the personal computer (PC).

The RTSDAS.vi software, developed for strain data acquisition and logging, was used for strain data collection. The user interface of the RTSDAS.vi is shown in the Figure 8. The user can enter the voltage excitation value in the "Vex" field, gage factor in the "GF" field, channel identification in the "channel" field, scan rate in the "scan rate" field, and the number of samples to be averaged per data point in the field "number of samples to average for each data point". The appropriate bridge configuration can be selected from the "Bridge Config" drop down list menu.

The date and time for data logging are obtained from the system clock and the user can specify the filename including the directory path for data logging. If the save option button is in the "DON'T SAVE" position data will not be logged to the file. For logging the data in a file, the save option button should be in the "SAVE" position. The "Strain Strip Chart" plots the strain values acquired in real time (Vijaynath et al. 1999).

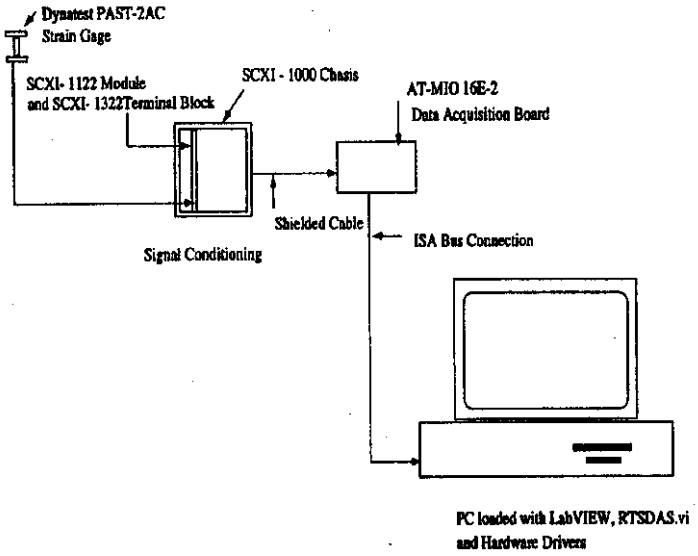

FIGURE 6: Schematic Representation of the Strain Data Acquisition System

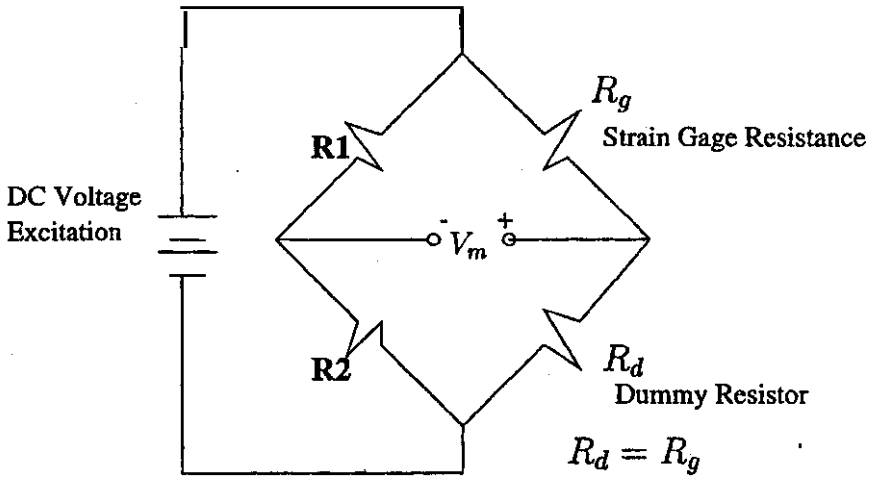

FIGURE 7: Bridge Configuration

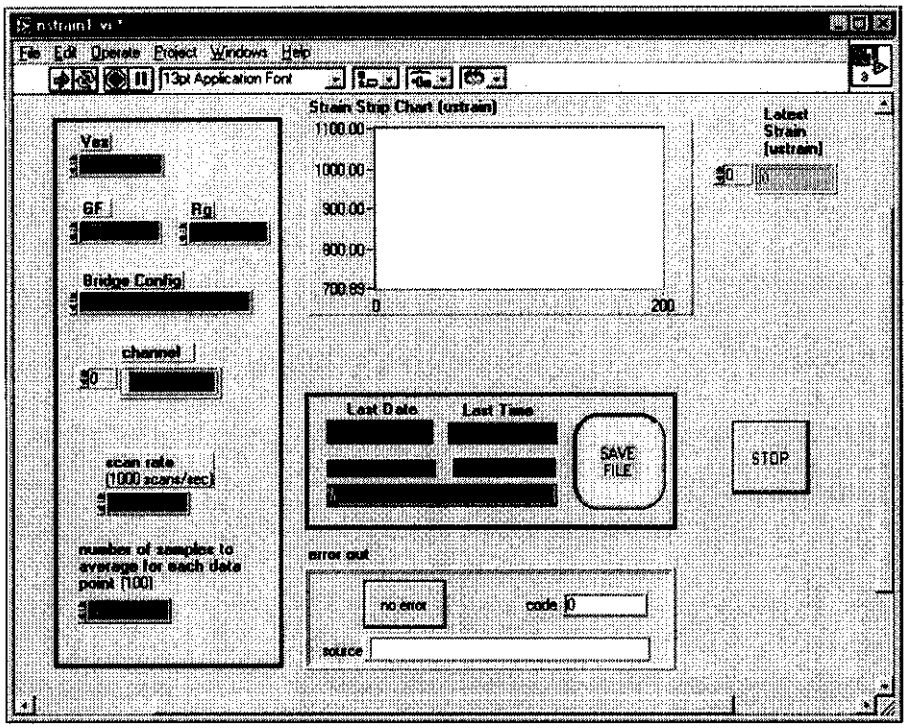

FIGURE 8: Graphical User Interface of RTSDAS.vi

2.3.6 Pressure Data Acauisition

A schematic of the pressure data acquisition instrumentation is shown in the Figure 9. The excitation voltage for the Geokon model 3500 earth pressure cell was provided with **an** external power supply unit. Pressure signals were channelized through the signal conditioning hardware consisting of a SCXI-1141 signal conditioning module, terminal block and SCXI-1000 chassis.

The data acquisition board (AT-MI0 16E-1) was connected to the signal conditioning module through a shielded cable. The data acquisition board was plugged in to the ISA slot of the PC mother board. The Pressure.vi software was used **for** pressure data collection. The user interface of the Pressure.vi was similar to that of RTSDAS.vi.

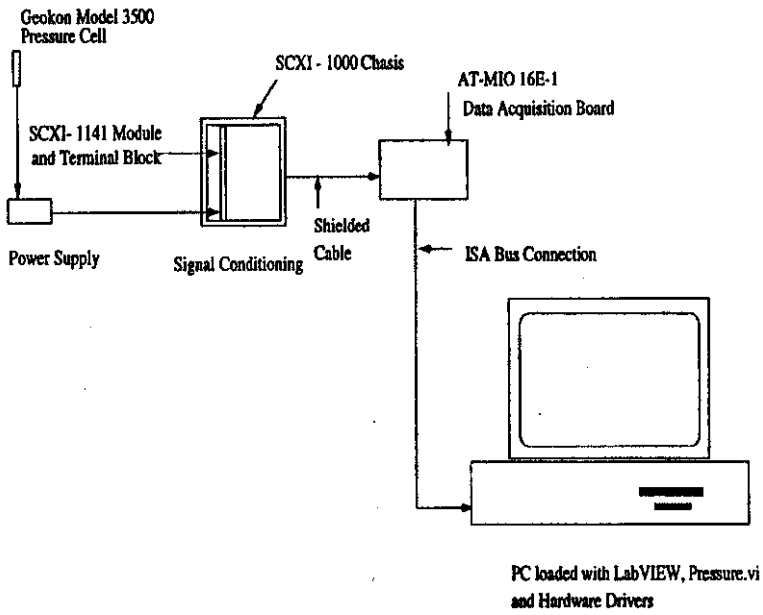

FIGURE 9: Schematic Representation Data Acquisition for Pressure Cell

CHAPTER 3

FATIGUE TESTS

3.1 Fatigue Tests

The fatigue tests of all SM-2A mixture beams used a third-point loading mode. The fatigue damage analysis (detailed in Chapter 5) was done by developing fatigue models from these test results. Two types of fatigue test beam were used in this study:

(i) In-situ beams sawed out of the south section (SM-2A (15) mixture) after completion of the test, and

(ii) Beams fabricated with SM-2A (15) loose samples collected during test section construction.

A typical fatigue test beam was 100 mm (4 in) wide, 75 mm (3 in) high, and 400 mm (16 in) long. The laboratory beams were fabricated in the Cox & Sons Kneading Compactor at the Material and Research Center of KDOT. In total, 16 laboratory beams and four in-situ beams were tested. Twelve in-situ beams were planned to be tested. However, most of the specimens were damaged in the trimming process and were unsuitable for testing.

Controlled stress type loading was selected with a haversine loading pattern of 0.1 sec duration without any rest period. The test temperature was 25° C (77° F). For each specimen, the deflection at the center of the beam after 200 cycles of load repetition was measured with a strain gage at the bottom fiber of the beam. The beam then was loaded repeatedly to full-depth cracking. The number of cycles needed to cause beam failure was recorded.

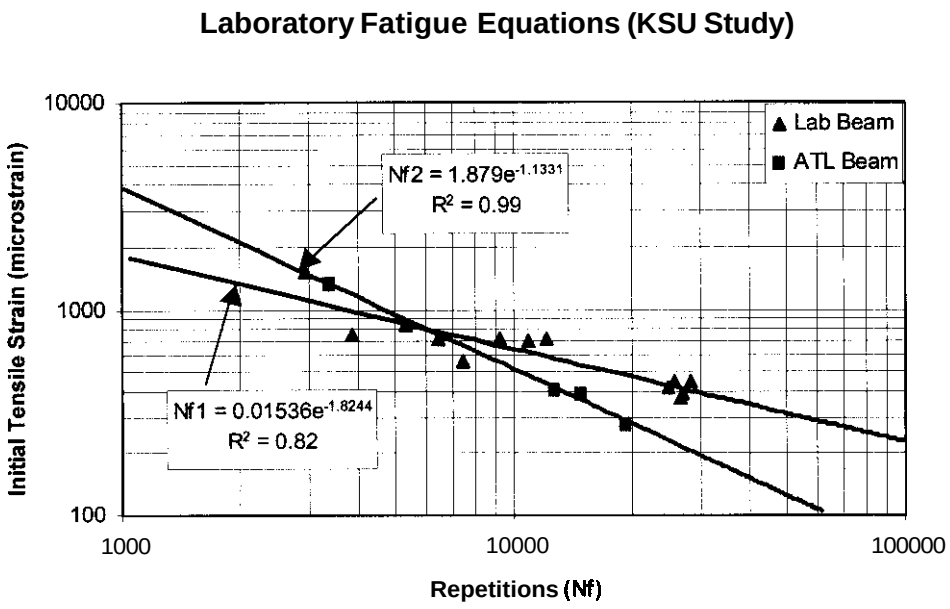

FIGURE 10: Laboratory Fatigue Equations

3.2 Fatigue Models

The following fatigue models were derived for the number of loading cycles (N_f) to fatigue failure and the initial tensile strain (ϵ_t) with regression analysis:

$$N_f = 0.01536\varepsilon_t^{-1.8244} \qquad R^2 = 0.82 \quad \textit{(Lab beams)} \qquad (i)$$

$$N_f = 1.879\varepsilon_t^{-1.1331} \qquad R^2 = 0.98 \quad \textit{(K-ATL beams)} \qquad (ii)$$

Figure 10 shows a plot of the above equations. It is to be noted that since the test section has already carried 80,000 repetitions of the K-ATL tandem axle, the fatigue curve obtained with the in-situ beams should be shifted to the left of the curve for the laboratory beams. Rather it intersects the lab beam equation indicating the following possibilities:

First, at the high tensile strain range the ATL beams can endure **a** relatively longer fatigue cycles

than the laboratory beams. This indicates that as the Superpave mixture materials become aged, the internal structure will be changed and will result in an increase in the elastic modulus. This will make the ATL beams last longer under fatigue cycles.

Second, the Superpave mixture materials will become more brittle when aged. This is why under relatively lower tensile strains the laboratory beams have a higher fatigue life than that of the ATL beams. This supports previous observations that the on-service pavement sections will have higher fatigue life than laboratory asphalt mixture beam samples.

CHAPTER 4

ANALYSIS OF PAVEMENT RESPONSE

4.1 Deflection Data Analysis

4.1.1 Falling Weight Deflectometer (FWD) Test

Deflection data was collected on each section at the strain gage and pressure cell locations (designated as Sta. 5+0, 10+0 and 15+0) with a Dynatest 8000 FWD after construction (before any loading was applied), after 40,000 repetitions and again after 80,000 repetitions. The first sensor was located at the center of the loading plate with six others at the Long term Pavement Performance (LTPP) sensor configuration (sensor spacing of 0", 8", 12", 18", 24", 36" and 60" from the center of load plate, respectively). Three drops of the FWD load were used for each of the target loadings of 40 and 67 kN (9 and 15 kips). The tests were conducted in a bi-directional mode i.e. from the east-west and then from the west-east direction on each section as shown in Figure 11. The strain gage and pressure cell readings were taken concurrently. The FWD tests were conducted at room temperature (about 22 "C).

4.1.2 Backcalculation of Laver Moduli

The FWD deflection data was analyzed using a modulus backcalculation computer program, EVERCALC, which was developed by the Washington Department of Transportation. A four layer pavement structure was used in the backcalculation: a Superpave mixture layer **(AC),** a base layer (AB-3), a subgrade layer (SG) and a stiff layer with an assumed modulus of 1,000 ksi. The effect of direction of testing was found to be very prominent and only results from the east- to-west tests were used in the analysis. In general, the backcalculation results were very satisfactory as evidenced by the

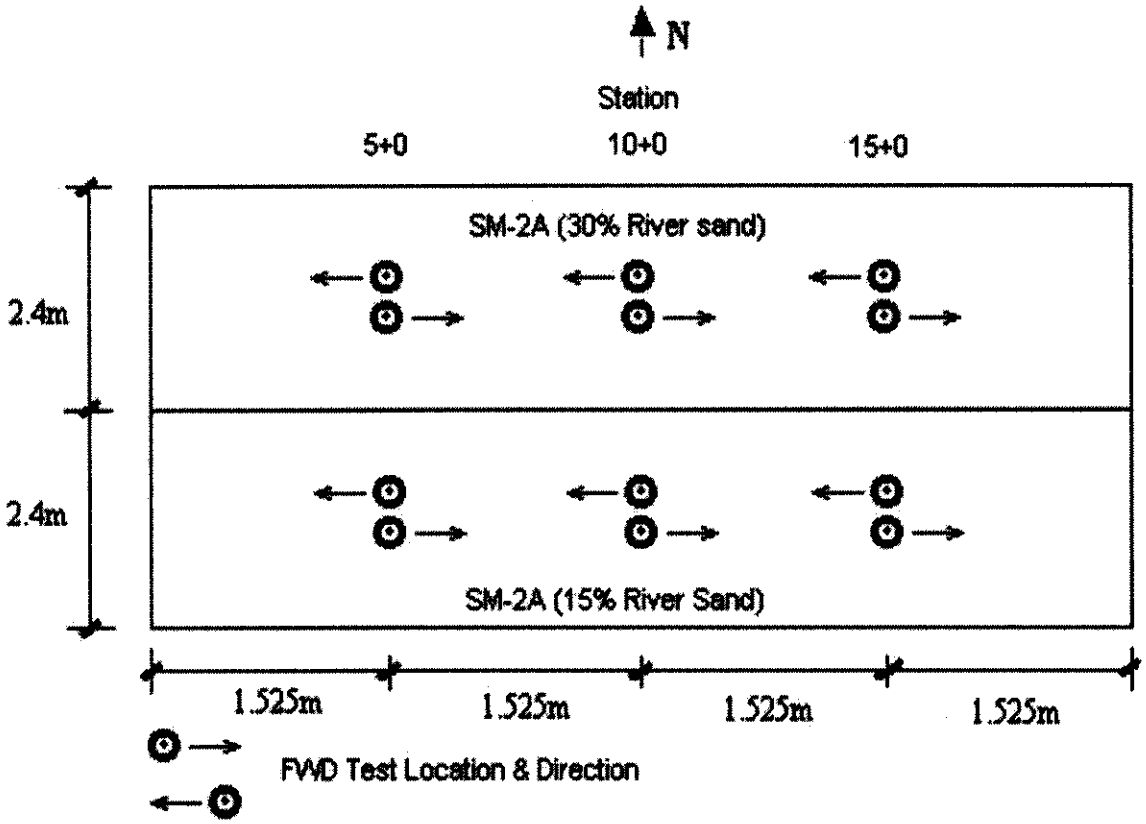

FIGURE 11: Falling Weight Deflectometer (FWD) Test Layout

root-mean-square (RMS) values in Table 2, which shown the backcalculated results based on the FWD data at the beginning ofwheel loading tests. On average, the SM-2A (15) mix had a slightly higher modulus (9%) than the SM-2A (30) mix. The moduli of the aggregate base and subgrade layers were essentially similar. Table **3** shows the backcalculated results based on the FWD data at 40,000 and 80,000 repetitions on Station 10+00.

TABLE 2: Backcalculated Layer Moduli (FWD data at beginning of wheel loading test)

Lane	Layer	Modulus (MPa)				
		Sta. 5	Sta. 10	Sta. 15	Std. Dev.	**Average**
South (SM-2A with 15% River Sand)	AC[a]	1640	1113	1378	264	**1377**
	AB	317	448	393	66	**386**
	SG	28	28	28	0	**28**
	RMS (%)	1.03	1.23	1.44	-	**-**
North (SM-2A with 30% River Sand)	AC[a]	1158	1440	1213	149	**1270**
	AB	372	431	393	30	**398**
	SG	28	28	28	0	**28**
	RMS (%)	**1.50**	**1.15**	**1.32**	**-**	**-**

"Temperature-correctedat **25** °C (77 **°F).**

TABLE 3: Backcalculated Moduli Results on Station 10+000 After Load Reuetitions

Lane	Layer	Modulus (MPa) under different load repetitions		
		0	40,000	80,000
South (SM-2A with 15% River Sand)	AC	1113	820	882
	AB	448	714	565
	SG	28	28	28
North (SM-2A with 30% River Sand)	AC	1441	379	579
	AB	431	1034	914
	SG	28	21	28

The asphalt layer moduli had decreased on the north section after 40,000 wheel loading repetitions. The change happened presumably due to internal damage. It is to be noted that this section showed the highest rutting. After 80,000 repetitions, the asphalt modulus remained almost the same as after 40,000 repetitions. The aggregate base modulus also increased with loading. It is possible that due to repeated load applications, stone-to-stone contact of the crushed stone base was enhanced and that resulted in higher modulus. The aggregate bade modulus on the north section was higher. It is to be noted that due to somewhat lower asphalt modulus on this section, higher stresses were applied on the aggregate base of this layer. Thus the modulus **of** the base layer on this section tended to be higher because of stress-sensitivity. It is well know that as the deviator stress increases, the modulus of granular material increases. The subgrade layer moduli remained relatively unchanged since no moisture fluctuation was allowed during the test.

4.2 Comparison of Computed and Measured Pavement Responses

The strain gage and pressure cell measurements were recorded during K-ATL wheel load application. First, the pavement surface was heated to about 49 °C (120 "F) with radiant infrared heat lamps. The temperature at the middle of the Superpave mixture layer was monitored with the thermocouples. The lamps were adjusted so that the temperature at the mid-depth location was 37.8 ± 1.1 °C (100 ± 2 "F) during wheel load applications. The load application was channelized directly over the gage locations i.e. the lateral position of the K-ATL tandem axle was not changed during testing. The selected wheel path location was such that half of the tandem axle assembly traveled on each section. Strain gage and pressure cell readings were taken for a few cycles of K-ATL loading initially (0 repetitions), for 100 cycles at 10,000 repetitions and for 50 cycles at 20,000 and 30,000 repetitions.

4.2.1 Pavement Response Under FWD Loading

It is well known that the FWD load is an impulse load with a 25 to **35** millisecond duration which is somewhat lower than typical interstate traffic wheel load duration. In order to compare the pavement responses measured from the strain gages and pressure cells under an FWD load and those computed from the backcalculated layer moduli using FWD data, responses from eight (8) strain gages and six *(6)* pressure cells were used. Figure **12** shows the typical response of a strain gage under FWD loading. It is noteworthy that since the interval between individual FWD load drops was only a few seconds, the strain gages did not have enough time to get back to the initial reading from the first FWD load drop to the next presumably due to pavement vibration caused by the FWD impulse load (Fig. 12). **A** longer pause after each FWD load drop would have been ideal for response data collection under FWD load. Similar trends were observed for the pressure cell readings.

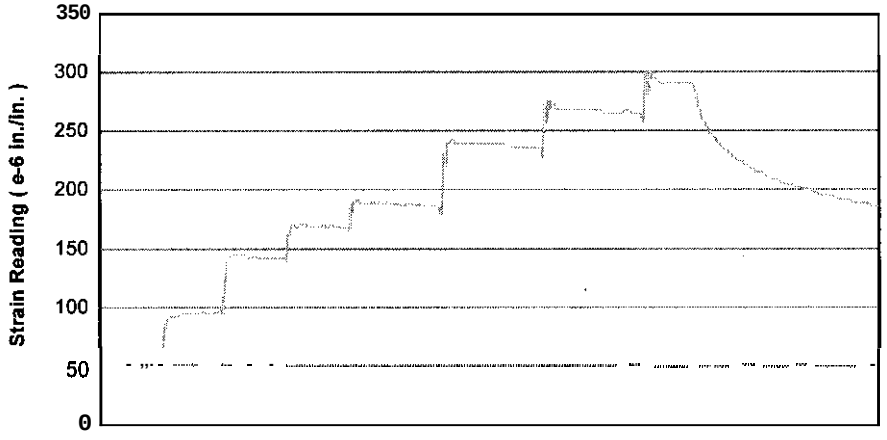

FIGURE 12: Typical Responses of Strain Gages Under Multiple Drops of FWD Loading

Table 4 shows the horizontal tensile strains at the bottom of the Superpave mixture layer and the vertical compressive stresses on the top of subgrade before load application, computed by ELSYM5. The layer moduli used in the "forward" response calculation process were backcalculated from the FWD data. Measured strains and stresses at the test locations are also shown in Table 4. The measured stresses and strains under the FWD loads are generally very close to those calculated by ELSYM5. The average ratios of the calculated strains to the measured strains for the north and south sections are 1.32 and 1.49, respectively. Excellent agreements were observed at some locations (Sta. 5+0 and Sta.10+0 on the south lane and Sta. 10+0 on the north lane) under all FWD loads. These results support the observations made earlier at LINTRACK (Ulldtz et al. 1996). The discrepancies observed at other locations are believed mainly due to the vibration created by the narrow load pulse of FWD, sensitivity of the gages and in general, simplified assumptions made for the pavement response calculations based on the multi-layer elastic theory. The relationship between measured and calculated tensile strains under FWD loading were compared using a linear regression analysis. The coefficient of determination was found to be very good ($R^2 = 0.72$, $n = 16$). The results indicate that despite limitations, the multi-layer elastic theory for the asphalt pavements is generally a good estimator of pavement responses.

The measured and calculated vertical compressive stresses on the south section corresponded very well (the average ratio was 0.90), hut higher discrepancies were observed on the north section presumably due to variation in the aggregate layer thickness. In general, measured vertical compressive stresses were higher than the calculated stresses at all station locations **as** well as on both sections. The SM-2A(15) had higher measured and calculated vertical compressive stresses at Sta. 10+0 than the north section presumably due to slightly lower as-constructed SM-2A layer modulus. The effect was

more pronounced at higher FWD target loads. Again, the ratio of calculated to measured vertical stresses are different for FWD tests done from different directions for the south section. It is believed that the stress-sensitivity of the granular materials might have played a part in it especially when the results corresponding to load drops of 40 kN and *67* kN are compared.

TABLE 4: Comparison of Calculated and Measured Pavement Responses Under FWD

Lane	Sta	FWD Load (kN)	Tensile Strain (micro-strain)			Vertical Stress (kPa)[a]		
			calc.	meas.	ratio	calc.	meas.	ratio
South (SM-2A with 15% River Sand)	15	40	197	101	1.95	26.9	26.3	1.02
	15	61	334	160	2.09	29.8	47.9	0.62
	10	40	188	182	1.03	18.9	18.0	1.05
	10	67	345	291	1.19	31.9	37.3	0.86
	5	40	233	245	0.95	20.5	17.0	1.20
	5	67	384	383	1.00	33.8	37.3	0.91
	10*	40	195	178	1.10	19.0	22.2	0.86
	10*	67	328	266	1.23	31.3	47.9	0.65
	Average				**1.32**			**0.90**
North (SM-2A with 30% River Sand)	15	40	187	124	1.51	17.0	24.7	0.69
	15	67	332	229	1.45	24.3	47.1	0.51
	10	40	185	134	1.38	17.4	18.1	0.96
	10	67	332	259	1.28	29.9	37.2	0.80
	5	40	217	136	1.60	19.8	24.0	0.83
	5	67	366	235	1.56	33.1	52.4	0.63
	10*	40	180	113	1.59	17.2	31.6	0.54
	10*	67	301	191	1.58	28.5	55.3	0.5 I
	Average		-		**1.49**			***0.69***

* testing from the other direction

4.2.2 Pavement Responses Under Wheel Loadings

Figures 13 and 14 show the typical pavement responses recorded by an asphalt strain gage and a pressure cell, respectively. It may be noted that the responses under wheel loadings and FWD loadings are totally different. The "rebound" during wheel loading is obvious since the gages were at "rest" (i.e. not excited by the vibration) due to longer rest periods between load cycles as shown in Figure 13. The two peaks in a cycle correspond to the passages of the axles of the K-ATL tandem wheel load assembly.

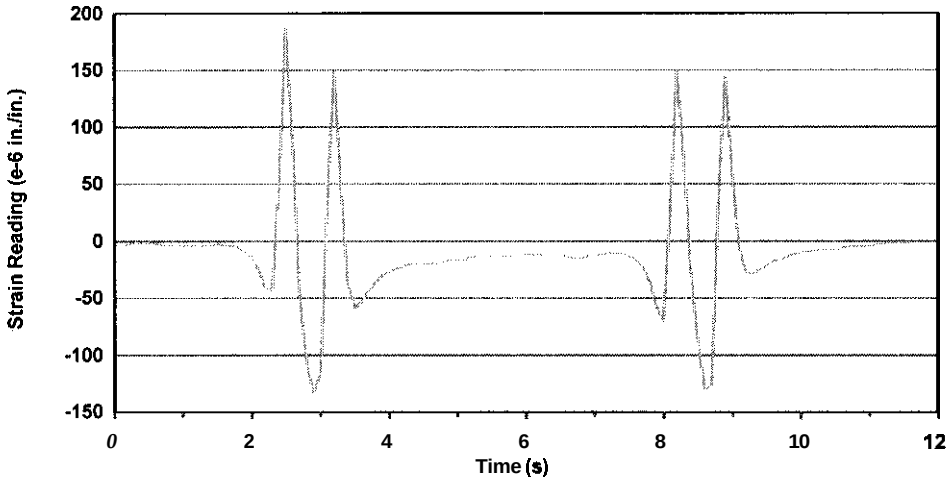

FIGURE 13: Typical Responses of Strain Gages Under Wheel Loading

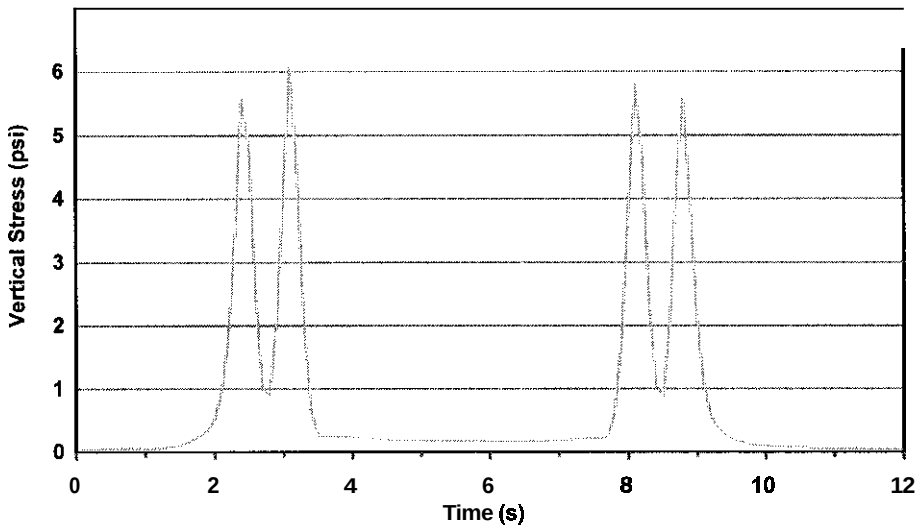

FIGURE 14: Typical Responses of Pressure Cells Under Wheel Loading

The calculated and measured pavement responses at the beginning of wheel loading have been tabulated in Table 5. It is to be noted that the **AC** layer moduli were corrected to the test temperature of **38 °C** (100 °F) using the LTTP temperature correction algorithm while computing the pavement responses. Results in Table 5 show that the measured tensile strains at the bottom of the **AC** layers were higher than the calculated values, and the discrepancy was greater for the vertical stress on the top of the subgrade. Part of the difference may result from the temperature correction of the **AC** layers moduli and some other known factors such as, idealized assumptions in the multi-layer elastic theory which may not be fully true in real world application. The south section with **SM-2A** (15) had higher tensile strain at the bottom of the Superpave layer and vertical compressive stress on the top of the subgrade than the north section with **SM-2A (30).** This is true for both the average and the individual locations (stations).

TABLE 5: Comparison of Calculated and Measured Pavement Responses at the Beginning of Wheel Loading

Lane	Sta	Tensile Strain (micro-strain)			Vertical Stress (kPa)		
		calc.	meas.	ratio	calc.	meas.	ratio
South (SM-2A with 15% River Sand)	15	161	**231**	**1.43**	**21.1**	52.0	**2.41**
	10	146	163	1.12	21.8	38.7	1.77
	5	200	289	1.45	23.2	34.2	1.48
	Average	**169**	**228**	**1.35**	**22.0**	**41.6**	**1.89**
North (SM-2A with 30% River Sand)	15	154	157	1.02	20.5	49.7	2.43
	10	150	172	1.15	20.7	36.0	1.74
	5	176	221	1.26	22.9	34.7	1.52
	Average	**160**	**183**	**1.14**	**21.4**	**40.1**	**1.88**

4.3 Progression Of Pavement Response Under Wheel Load Repetition

Table ***6*** lists the summary statistics of the measured tensile strains and vertical compressive stresses at K-ATL tandem axle repetitions of 0, 10,000, 20,000 and 30,000. In general, the tensile strains were found to increase with increasing wheel load repetitions. On average, the change was not very prominent, and may be well within the variability of the strain measurements. The maximum coefficient of variation of the strain gage readings was about 35 percent with a range of 9 to 35 percent. Much lower coefficients of variation **(3** to 5 percent) were observed for the vertical compressive stress measurements.

The results showed that the south section (SM-2A with 15 percent river sand) had higher

average tensile strain and vertical compressive stress than those on the north section (SM-2A with 30 percent river sand). The tensile strains appeared to increase with increasing wheel load repetitions. This may indicate decreasing AC layer moduli with increasing wheel load repetitions due to internal damages although no surface cracking was visible up to 30,000 repetitions. The vertical compressive stresses increased slightly on the south section, presumably due to a change in the Superpave layer thickness. However, the vertical compressive stresses on the north section decreased steadily with increasing number of wheel load. Some of these results tend to agree with the earlier results obtained in a TxMLS test (Chen et al. 1999).

The variations of the tensile strain and vertical compressive stress on both sections were quite consistent with the pavement performance. As shown in Figure 15, after 30,000 repetitions of the K-ATL tandem axle, both sections had developed comparable amount of rutting (about 11.5 mm) when measured from the original profile. However, the shapes of the rutted profiles are completely different. Most of the rutting on the south section was due to consolidation of the Superpave and/or other layers since little flow of the SM-2A layer material was evident. On the other hand, the north section had a large shear flow of the SM-2A layer material indicating a lack of stability, and most of the rutting happened due to this phenomenon. Thus, it appears that the Superpave mixture containing a large amount of river sand would be susceptible to plastic shear flow even when very high in-place density is achieved. The detailed rutting analysis will be described later.

TABLE 6: Change of Pavement Response with Wheel Load Repetitions

Lane	Sta		(micro-strain) @ _load cycles				(kPa) @_load cycles			
			0	10,000	20,000	30,000	0	10,000	20,000	30,000
South (SM-2A with 15% River Sand)	15	Mean	231	256	260	270	52.0	55.3	56.6	54.4
		C.V.	11.8	15.8	12.9	34.6	36.5	25.5	22.7	37.2
		Range	180~292	150~285	195~319	209~324	48~56	51~59	52~61	49~59
		n	100	100	32	20	28	28	35	34
	10	Mean	163	162	159	146	38.7	39.8	41.1	40.0
		C.V.%	10.3	10.6	11.4	21.3	18.6	28.9	37.9	33.1
		Range	135~207	120~200	120~190	108~179	37~41	36~42	37~44	33~43
		n	61	103	32	47	16	28	36	34
	5	Mean	289	326	334	343	34.2	30.5	30.8	30.3
		C.V.%	9.9	9.0	9.4	11.1	35.8	20.0	31.0	31.0
		Range	251~337	268~377	285~400	305~423	32~37	29~32	28~32	28~33
		n	6	92	32	20	32	16	36	36
	Average		**228**	**248**	**251**	**253**	**41.6**	**41.9**	**42.8**	**41.5**
North (SM-2A with 30% River Sand)	15	Mean	157	157	160	171	49.7	45.6	43.7	39.3
		C.V.%	15.1	14.0	12.7	11.1	25.5	30.3	24.8	22.0
		Range	106~207	116~207	116~189	126~191	47~52	43~50	41~46	37~43
		n	94	100	32	20	18	28	34	34
	10	Mean	172	178	179	204	36.0	35.0	33.9	32.4
		C.V.%	15.2	14.6	15.9	20.3	22.0	21.4	32.4	20.7
		Range	127~224	128~229	132~231	157~242	34~38	32~37	32~36	31~34
		n	99	104	35	44	18	28	40	34
	5	Mean	221	233	234	239	34.7	25.3	27.4	27.5
		C.V.%	10.8	11.3	10.2	11.5	27.6	28.2	31.0	26.2
		Range	111–285	150–285	181–274	180–290	32–37	23–28	25–30	25–30
		n	104	100	35	20	28	28	36	36
	Average		**183**	**190**	**191**	**205**	**40.1**	**35.3**	**35.0**	**33.1**

a. SM-2A with 30% Sand

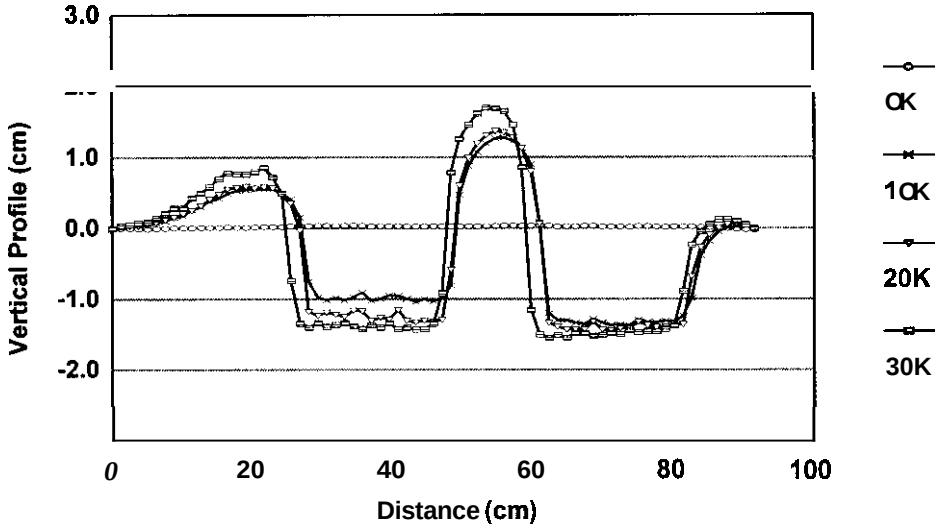

b. SM-2A with 15% Sand

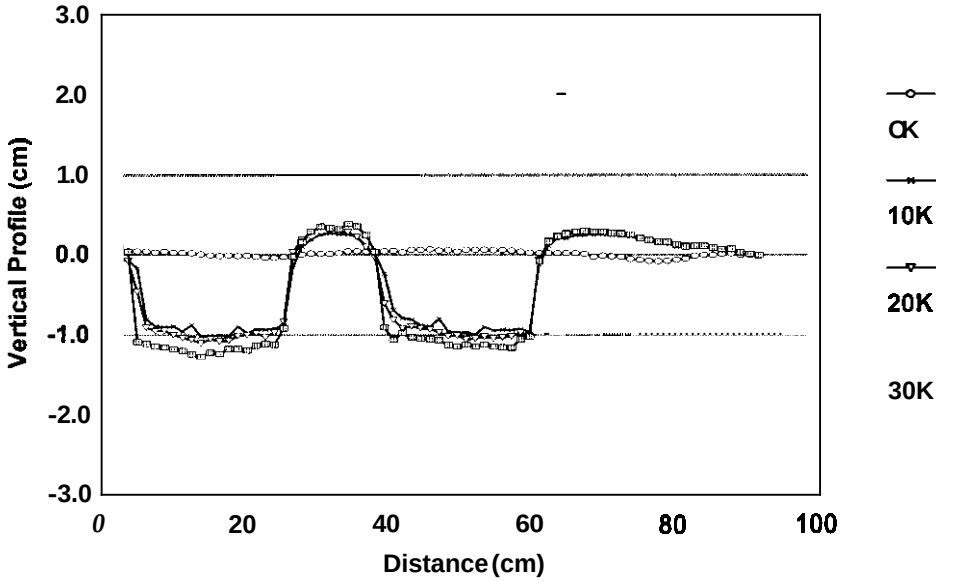

FIGURE 15: Rutting Observed on the Superpave Sections

CHAPTER 5

PAVEMENT DAMAGE ANALYSIS

5.1 Fatigue Damage Analysis

The fatigue damage analysis was done by developing fatigue models through laboratory fatigue testing of the SM-2A beams using a third-point loading mode. Two types **of** fatigue test beam were used in this study:

(i) In-situ beams sawed out of the south section (SM-2A with 15 percent sand) after completion of the test, and

(ii) Beams fabricated with SM-2A loose samples collected during test section construction. As described in Chapter 3, the following fatigue equations has been obtained:

$$N_f = 0.01536\varepsilon_t^{-1.8244} \qquad R^2 = 0.82 \quad \textbf{(Lab beams)} \qquad (3\text{-}1)$$

$$N_f = 1.879\varepsilon_t^{-1.1331} \qquad R^2 = \textbf{0.98} \quad \textbf{(K-ATL beams)} \qquad (3\text{-}2)$$

The fatigue models shown in Equations 3-1 and 3-2 needed to be transferred to the field condition when doing in-situ fatigue damage analysis. A transfer factor of 100 was selected based on a previous study of the Superpave mixtures in Kansas (Kaldate and Hossain 1998).

The pavement damage caused by the repetitions of a given load can be expressed as the ratio of the actual to the allowable number of load applications. This ratio is referred to as the damage ratio. To accumulate the damages caused by various axle loads and configurations, the Miner's cumulative

damage hypothesis is widely used. Failure is expected when the cumulative damage ratio, D_f, equals or exceeds 1.0 or 100 percent, according to the following expression (Ali and Tayabji 1998):

$$D_f = \sum_{i=1}^{k} \frac{n_i}{N_{fi}} \qquad (5\text{-}1)$$

where k = number of loadings groups;

n_i = cumulative number of repetitions of load group i; and

N_{fi} = allowable number **of** repetitions to failure of load group i.

Table 7 shows the fatigue damage ratios computed using Equations (i), (ii) and (iii) and a transfer factor of 100 for the Superpave mixture on the south section (SM-2A with 15 percent sand). The damage ratios ranged from 1.3 percent to 10.6 percent with an average value of 5.5 percent. The results indicate no significant fatigue damage after 80,000 repetitions of the 150 kN (34-kip) K-ATL tandem axle. Further validation of this observation was made by calculating fatigue damage ratios on both sections using the Asphalt Institute (AI) fatigue model:

$$N_f = 0.0796\varepsilon_t^{-3.291} E_{ac}^{-0.854} \qquad (5\text{-}2)$$

where: N_f = allowable number of repetitions to failure;

e, = tensile strain at the bottom of the AC layer; and

E,, = modulus of the AC layer.

Table 6 also shows the computed damage ratios using the AI fatigue model, and it ranged from 0.02 percent to 0.3 percent. The AC moduli were obtained from the backcalculated values shown in

Table **2.** On the north section (SM-2A with 30 percent sand), the average damage ratio computed from the AI fatigue model was only 0.03 percent.

These results imply that the test sections have undergone no significant fatigue damage up to 80,000 repetitions. Visual observations at the surface and after trenching have confirmed this assessment.

Section	Station	Fatigue Damage Ratio (after 80,000 loading cycles)			Rutting Damage Ratio (after 80,000 loading cycles)	
		Lab Model	K-ATL Model	**AI** Model	Original	"Enlarged"
South (SM-2A with 15% sand)	5+0	0.054	0.106	0.00033	0.051	1.142
	10+0	0.013	0.045	0.0002	0.022	0.487
	15+0	0.034	0.079	0.0010	0.027	0.591
North (SM-2A with 30% sand)	5+0	/	/	0.0007	0.041	0.796
	10+0	/	/	0.0003	0.041	0.802
	15+0	/	/	0.0002	0.015	0.313

5.2 Rutting Damage Analysis

Miner's hypothesis was also followed in the rutting damage analysis. The Asphalt Institute (AI) permanent deformation (rutting) model was selected to compute the rutting damage ratio. This model relates the vertical compressive strain at the top **of** the subgrade ***(E,)*** to the number of load repetitions to failure due to permanent deformation (N_p), in the form of the following expression (Ali and Tayabji 1998):

$$N_p = 1.365 \times 10^{-9} \varepsilon_c^{-4.477} \qquad (5\text{-}3)$$

Failure is defined as the development of 15 to 19 mm (½ to 3/4 in) rutting or in other words, the cumulative permanent deformation damage ratio of 100 percent would correspond to this rutting. In this study, the critical response measured at the top of subgrade was vertical compressive stress. Therefore, the theoretical vertical compressive strain computed by an elastic multi-layer program, ELSYM5, was used. The backcalculated layer moduli corresponding to the FWD tests at 0, 40,000 and 80,000 repetitions, were used to characterize the layer moduli. The computed rutting damage ratios are shown in Table 7. Very negligible damage ratios (average 3.3 percent) were obtained on both test sections. According to the rutting failure criteria of 15 to 19 mm rut depths for 100 percent cumulative damage ratio, the computed average damage ratio would translate to 0.5 to 0.6 mm rut depths on these sections. However, the observed rut depths after 80,000 tandem axle repetitions were about 28 mm and **17** mm, respectively, on the north and the south sections.

Previous studies *(Ullidtz et al. 1996; Ullidtz 1998)* have shown that the measured vertical strain/stress on the top of subgrade is generally twice the calculated values based on the elastic layer theory. In this experiment, the average ratio of the measured compressive stress by the pressure cell at the top of the subgrade to the calculated value was about 1.9. If the same ratio is taken for the vertical strains, the calculated vertical compressive strain at the top of the subgrade should be "enlarged" using a factor of two. The resulting rutting damage ratios then tend to match reasonablely with the in-situ rut depths (Table 7). The average enlarged damage ratios were 74 and 64 percent, respectively, on the south and north sections. According to the AI permanent deformation criteria, these average, enlarged damage ratios will contribute to the rut depths of 11 to 14 mm on the south section and 10 to12 mm on

the north section after 80,000 repetitions. While these results still do not match exactly with the in-situ observation, it is clear that they are getting close. Two reasons were thought to account for the observed discrepancies: (i) Initial consolidation (rutting) of the **AC** and other layers; and (ii) Transferability of the AI permanent deformation model. The first observation will be discussed in details in the following sections.

CHAPTER 6

RUTTING DAMAGE ANALYSIS BASED ON DEFORMATION AREA

6.1 Definition of Rut Area

The rutted profiles of the test sections at the middle location (Sta. 10+0) were analyzed in details. Figure 16 shows the definition of the areas in the vertical profile. On this figure, area below the "original" transverse profile is nothing but "depression" due to consolidation/densification and due to loss of the **SM-2A** material resulting from shear flow. The shear flow material is deposited in the "heave" area. Thus, the total volumetric change of a mixture is the consolidation or densification, which in terms of rut area (as defined in Figure 16), is the area of depression minus the area of heave.

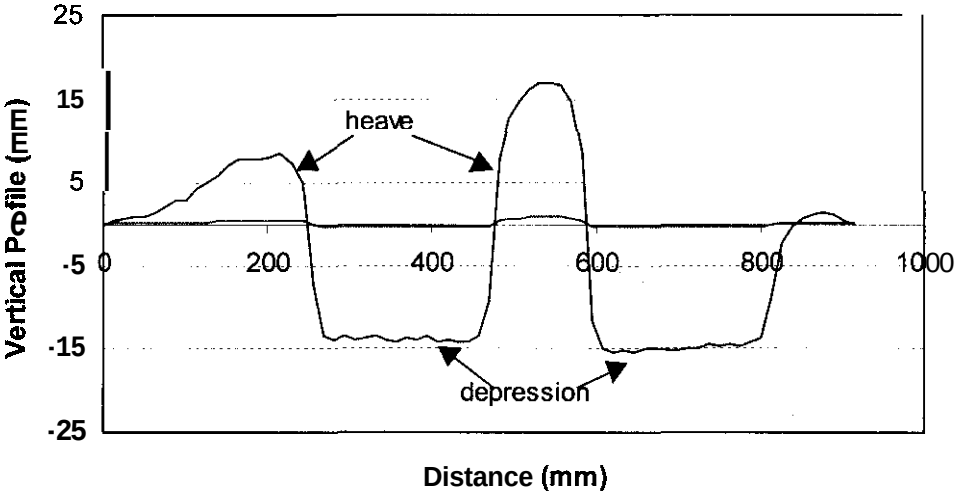

FIGURE 16: Rutting Area Definition

6.2 Analysis of Rut Area

Figure 17 shows the area calculations on both sections with increasing number of load repetitions. The depression in this figure includes both densification and loss of SM-2A material resulting from the shea flow. Several observations can be made from this figure:

(i) the area of depression was generally bigger than that of heave on both sections;

(ii) the area of heave on the north section (30) was almost twice the area on the south section (15);

(iii) the area of heave on both sections remained almost constant after initial several thousand load repetitions (10,000 for the south section and 30,000 for the north section); and

(iv) the area of consolidationidensifcation kept **on** increasing until 50,000 load repetitions on the south section and 80,000 load repetitions on the north section.

On the north section, the heave area was about 27 percent of the total rut area (heave area plus depression area) after 80,000 load repetitions, and the densification area was about 45 percent. Twenty five percent consolidation happened **on** the north section after the initial 10,000 load repetitions. On the south section, the heave area accounted for 15 percent of the total deformation area, and the consolidationidensifcation area accounted for about 74 percent of the total area at the end of the experiment. After the initial 10,000 load repetitions, the south section had 43 percent area due to consolidation. It is, therefore, concluded that most of the rutting on the south section was due to consolidation of the SM-2A and/or other layers since little flow of the SM-2A layer material was evident. On the other hand, the north section had a large shear flow indicating a lack of stability, and most of the rutting happened due to this phenomenon. The consolidation areas among the total deformation areas on both sections were quite large and uncommon when high in-place densities, such as those achieved in this study, are obtained. In this experiment, this happened mainly due to the high

test temperature (about **38** "C) and probably due to unstable pavement materials, e.g., **SM-2A** with high river sand content and AB-3 with high fine content, used in construction of the sections.

South (SM-2A with 15%Sand)

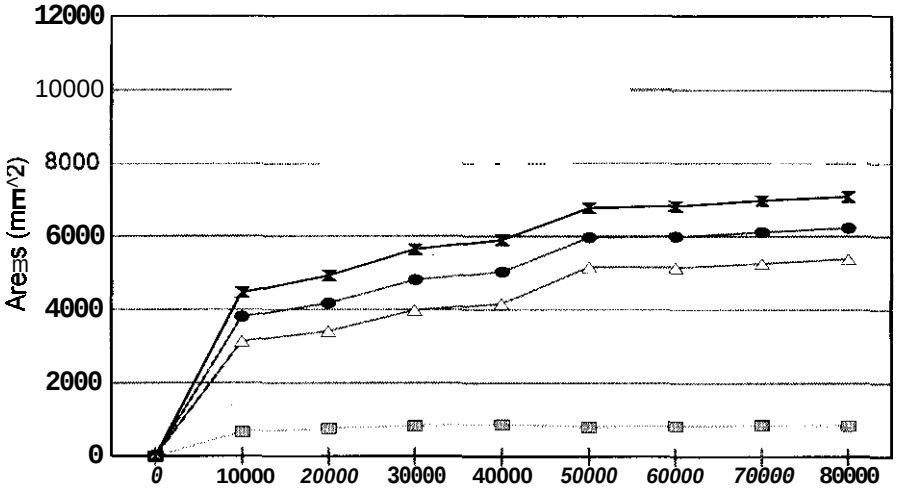

North (SM-2A with 30%Sand)

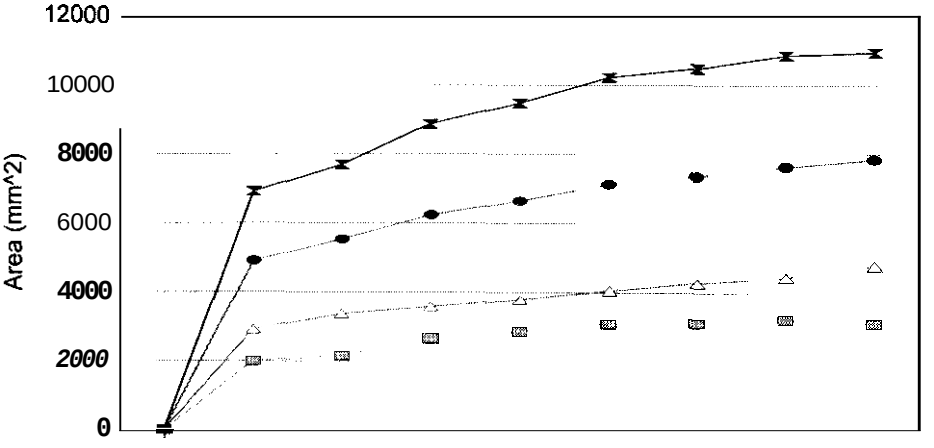

If the initial rut depth is taken mainly due to consolidation, which is about 25 percent on the north section and 43 percent on the south section, respectively, the final average rut depths would have been about 21 mm (0.82-in) and 10 mm (0.39-in) on the south and north section, respectively. These figures tend to match closely with the rut depths of 11 to 14 mm on the south section and 10 to 12 mm on the north section, previously obtained from the AI permanent deformation model.

CHAPTER 7

ANALYSIS OF PAVEMENT TEMPERATURE AND ROUGHNESS

7.1 Pavement Temperature Measurements

As mentioned earlier, pavement temperature was measured at each location by four thermocouples: one at the middle of the SM-2A layer, one at the bottom *of* SM-2A layer, one at the middle *of* the aggregate base, and one at the top of the subgrade.

The overall average temperature at the middle **of** SM-2A layer was 35.9' C (96.7° F) with a standard deviation of 2.2° C (4.0° F) on the South section and 35.9" C (96.6° F) with a standard deviation of 3.0° C (5.5° F) on the north section throughout 80,000 repetitions. This results indicate that the temperature control system did not work very accurately in controlling the mid-depth temperature of Superpave mixture of 37.8 ± 1.1° C (100 ± 2° F), but it appears to be accurate enough for all practical purposes. Future test should pay more attention to this point. The temperature distribution across pavement structure were shown in the Figure 18. This distribution appears to be linear.

7.2 Analysis of Longitudinal Profile

Longitudinal profiles were measured using Dipstick at the end of each 10,000 repetitions in this study. RoadRuf, developed by the University of Michigan Transportation Research Institute (UMTRI), was used to interpret the resultant profile data. Table 8 shows the computed International Roughness Index (IRI) at each 10,000 repetitions on both section. It is to be noted that the length of each test section was only 6.1 m (20 ft) and there is a possibility of profile misrepresentation by Dipstick measurements due to 1 foot interval. However, the overall trend does give **an** indication of the roughness development through out the load repetitions. After 80,000 repetitions, the IRI value increased from 3.05 m/km (193

idmi) to 4.20 m/km (266 in/mi) on the North section, and from 2.87 m/km (182 idmi) to 3.76 m/km (238 idmi) on the south section. Rutting was more severe on the North section, and the IRI values do show that.

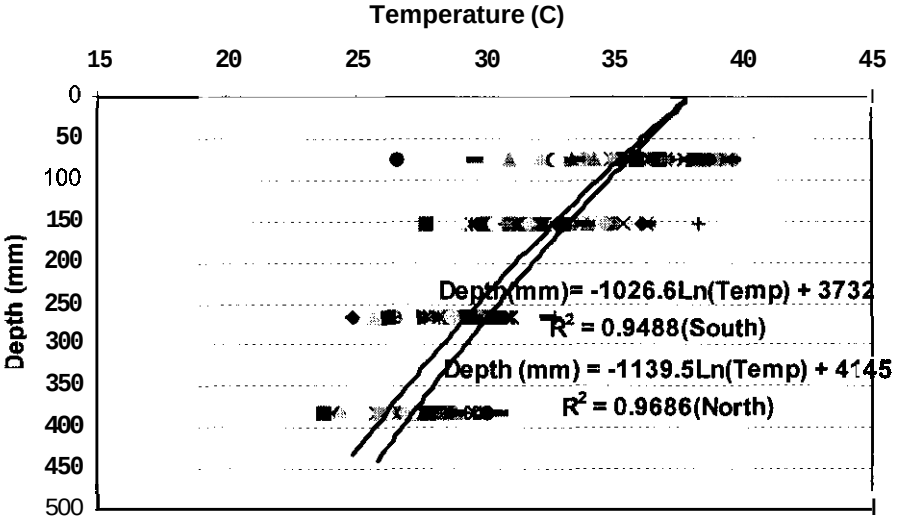

FIGURE 18: Temperature Distribution on Superpave Test Sections

TABLE 8: International Roughness Index Development on the Superpave Test Sections

No. of Repetitions (x1000)						
	Fore Dir.	Back Dir.	Average	Fore Dir.	Back Dir.	Average
0	3.50	2.60	3.05	3.17	2.70	2.94
10	2.46	3.71	3.09	2.64	2.92	2.78
20	2.32	3.35	2.83	2.64	2.95	2.79
30	2.19	8.33	5.26	2.65	3.16	2.90
40	2.13	3.84	2.98	2.23	3.00	2.60
50	2.48	3.85	3.17	3.50	2.97	3.24
60	2.41	3.98	3.19	4.18	2.90	3.54
70	3.01	4.59	3.80	3.96	3.00	3.47
80	3.14	4.99	4.20	4.07	3.44	3.76

CHAPTER 8

ANALYSIS OF RELATIVE PAVEMENT DAMAGE

8.1 Introduction of Equivalent Axle Load Factors

As mentioned earlier, the relative damage of the test sections due to different axle loads and configurations were studied by loading the test sections under six different combinations of axle load and configuration. The pavement responses were measured for more than 30 repetitions for each of the following axle loads and configurations:

Axle Type	Load (kN)
Single	80, 90 & 98
Tandem	144, 150 & 160

The relative pavement damage was estimated through calculations of the Equivalent Axle Load Factors (EALF's).

An EALF is defined as the *damage per pass* to a pavement by the axle in question relative to the damage per pass of a standard axle load, usually the 80 kN (18 kip) single axle load (Huang 1993). The EALF value for any given load can be expressed as (Yoder and Witczak 1995):

$$EALF = \left(\frac{\varepsilon_j}{\varepsilon_s}\right)^c \qquad (8\text{-}1)$$

where, ϵ_j is the tensile strain due to the jth vehicle, ϵ_s is the tensile strain due to the standard vehicle, and c is a constant. The c value typically varies from 3 to 6 and can be determined experimentally as the power of the fatigue equation or empirically.

8.2 Pavement Relative Damage

Typically, the fatigue test results of the asphalt concrete are expressed in terms of the number of repetitions to failure as a function of the initial tensile strain at the bottom fiber of the beam ***(Yoder and Witczak 1995):***

$$N_f = K(\frac{1}{\varepsilon})^c \qquad (8\text{-}2)$$

where, E is the maximum tensile strain at the bottom of asphalt beam and K and c are the regression constants.

In the mechanistic method of pavement design, when the fatigue cracking failure criterion is used, the c value is taken as *four* resulting in the well-known "Fourth Power" damage law. The EALF can then be determined as follows ***(Huang 1993):***

$$EALF = \left(\frac{\varepsilon_x}{\varepsilon_{18}}\right)^4 \qquad (8\text{-}3)$$

where, ϵ_x is the tensile strain at the bottom of asphalt layer due to a given axle load and ϵ_{18} is the tensile strain at the bottom of the asphalt layer due to an 80-kN (18-kip) axle load.

Equation (8-3) is valid only for the single axles. For tandem or tridem axles, ϵ_{18} should be replaced by the responses under applicable standard tandem or tridem axles. For tandem axle, 144kN (32.5 kip) can be taken as the standard axle because according to AASHTO, the EALF value **of** this axle is very close to 1.00 (same as 18kip/80 kN on a single axle). The EALF values determined by Equation (viii) are known to check favorably with the AASHTO load equivalency factors ***(6).*** However, many factors such as, the type of pavement, thickness or structural number, axle configuration, the terminal condition at which the pavements is considered failed etc., are all needed to be considered when computing AASHTO EALF's.

The c values obtained in this study, from Equations *(i)* and *(ii)*, were 1.8244 and 1.1331 for the lab beam and the K-ATL beam, respectively. In a previous study in Kansas, the c value was found to be

1.766 and 1.397 for the 19 mm (SM-2C) and the 12.5 mm (SM-1B) coarse Superpave mixtures, respectively (Kaldate and Hossain 1998). Therefore, the value of c for the Superpave mixtures may be significantly lower than the traditional asphalt mixtures which are assumed to follow the "Fourth Power" damage law. In other words, the Superpave mixtures appear to be less susceptible to fatigue damage than the traditional mixtures. It is believed that the better aggregate structure and higher binder content used in the Superpave mixtures contribute to the higher fatigue damage resistance than the traditional mixtures.

8.3 Comparison of the Equivalent Axle Load Factors (EALF)

The EALF factors were computed from the average measured tensile strains at the bottom of the AC layers using c values from the (i) lab beam fatigue equation (Equation (i)), (ii) K-ATL beam fatigue equation (Equation (ii)), and (iii) the "Fourth Power" law (Equation (viii)). The tensile strains under the K-ATL 80 kN (18 kip) single axle and 144 kN (32.5 kip) tandem axle loads were taken as the responses under the standard axles when using Equation (viii). The computed EALF values are shown in Table 8. The table also shows the corresponding AASHTO EALF's obtained from the 1993 AASHTO Pavement Design Guide (AASHTO 1993). In general, the EALF values varied from station to station. The AASHTO values showed the highest EALF's for the single axle loads (20 kip and 22 kip). For tandem axles, the K-ATL model resulted in the highest EALF values for the 160 kN (36 kip) tandem axle. The "Fourth Power" model gave EALF's lesser than or equal to the AASHTO values, but had higher values at Sta. 5+0 and 15+0 for the 150-kN (34-kip) tandem axle. Although the K-ATL and lab beam models showed similar results, large differences with the AASHTO and the "Fourth Power" models were observed for the axle loads and configurations. Because of the "edge" effect, the values obtained in the middle station, Sta 10+0, were used for comparison between the EALF's obtained in this study and the AASHTO load equivalency factors. It appears that for this Superpave mixture test section (SM-2A with 15 percent sand), AASHTO

EALF's will overestimate the computed Equivalent Single Axle Loads (ESAL's) by about 29 to 80 percent for the single-axle loads and by about 34 to 68 percent for the tandem axle loads. The upper ends of the ranges were obtained at higher load levels for both axle configurations.

TABLE 9: Comparison of Eauivalent Axle Load Factors

Load (kN)	Axle Number	Axle Spacing (mm)	Station	EALF (based on 80kN single axle and 145kN tandem axle loads)			
				AASHTO	Fourth Power	K-ATL	Lab Beam
80	Standard	-		1.000	1.000	1.000	1.000
89	1	/	5+0	1.510	1.302	1.078	1.128
			10+0	1.510	1.419	1.104	1.173
			15+0	1.510	1.176	1.047	1.077
98	1	/	5+0	2.180	1.827	1.186	1.316
			10+0	2.180	2.006	1.218	1.374
			15+0	2.180	1.403	1.101	1.167
145	Standard	-	-	1.000	1.000	1.000	1.000
151	2	1270	5+0	1.095	1.361	1.091	1.151
			10+0	1.095	1.090	1.025	1.040
			15+0	1.095	1.228	1.060	1.098
160	2	1270	5+0	1.380	1.387	1.097	1.161
			10+0	1.380	1.113	1.031	1.050
			15+0	1.380	1.376	1.095	1.157

CHAPTER 9

CONCLUSIONS AND RECOMMENDATIONS

9.1 Conclusions

The following conclusions can be drawn from the preliminary results of this study:

(i) The measured vertical stresses on the top of the subgrade and tensile strains at the bottom of the AC layer due to FWD loads are generally very close to those calculated by ELSYM5.

(ii) Under K-ATL wheel loads at *the* beginning, the measured tensile strains and vertical stresses on both sections were higher than those calculated by ELSYM5 indicating that the theoretical responses are somewhat conservative estimates.

(iii) The tensile strains at the bottom of the AC layers increased with increasing number of wheel load repetitions, and the measured vertical stresses remained relatively constant.

(iv) After 30,000 repetitions of the K-ATL tandem axle, both sections had developed comparable amount of rutting (about 12mm) when *measured from* the *original profile*. However, the shapes of the rutted profiles are completely different on these sections - the rutting on the south section appeared to be due to consolidation of the SM-2A and/or other layers, whereas a large shear flow of the SM-2A layer material on the north section was evident. This indicates that the Superpave mixtures containing a large amount of river sand would be susceptible to plastic shear flow.

(v) The cumulative fatigue damage ratios on the Superpave test sections in this study varied from 0.013 to 0.106 with an average value of 0.055 after 80,000 repetitions of the 150-kN (34-kip) K-ATL tandem axle. This indicates very little fatigue damage on these sections which is consistent with the visual observations made at the surface and after trenching of the test sections.

(vi) The permanent deformation (rutting) damage ratios, calculated using the theoretical vertical compressive strains at the top of the subgrade and the AI permanent deformation model, did compare well with the in-situ rutting when the initial densification of the Superpave mixtures was taken into account.

(vii) A detailed analysis based on the rutted vertical profiles showed that on the north section, most of the rutting happened due to shear flow of the SM-2A material. On the south section, most of the rutting was due to consolidation of the SM-2A and/or other layers since little flow of the Superpave mixture was evident.

(viii) A study of relative damage due to different combinations of axle loads and configurations showed that the AASHTO load equivalency factors were much higher than those obtained in this study. The discrepancy is greater at higher load levels for both axle types. However, the EALF's computed from the "Fourth Power" law are more or less similar to the AASHTO EALF's.

9.2 Recommendations

The results of tlns study show that if the Superpave layers are to be placed on dense graded aggregate base (AB-3), the base should be compacted very well. A 95 percent compaction is recommended for such a case, and could be easily achieved because of high fine content in ***AB-3.*** The amount of river (natural) sand should be limited in the Superpave mixture. Currently KDOT is proposing in the revised specifications for the Superpave mixture (M-230-R9) that natural sand shall have an uncompacted void content "U" value of less than 42.0. The required "U" value at the time of test section constructed for this study was 40.0. Also, for all Superpave mixtures to be used on the traveled way, M-230-R9 specifies that the quantity of natural sand shall not exceed 35 percent. This percentage of natural sand appears to be very high for the Superpave mixtures, especially on routes with higher volumes of truck traffic (accelerated loading).

Considering packing of the aggregates in dense gradation, the natural sand content should be a function of the nominal maximum aggregate size of the blend. The results of this study show that for 12.5 mm nominal maximum aggregate size, natural sand content should be well below 30 percent, preferably 15 to 20 percent, if the mixture is to be used on high traffic routes, even as overlays. For 19.0 mm nominal maximum aggregate size, slightly higher natural sand content (20 to 30 percent) could be permitted given the fact that the stone-on-stone contact is better for higher size aggregates.

REFERENCES

AASHTO. *Guidefor Design of Pavement Structures.* AASHTO, Washington, D.C., 1993.

Ali, A.H. and Tayabji, S.D. *Evaluation of Mechanistic - Empirical Performance Prediction Models for Flexible Pavements.* In Transportation Research Record No. 1629, Transportation Research Board, Washington, D.C., 1998.

Baker, H.B. and Buth, M. R. *Load Response Instrumentation Installation and Testing Procedures:* Minnesota Road Research Project. *Proceedings of the 4th International Conference on Bearing Capacity of Roads and Airfields,* Vol. 2, pp. 1371 - 1383, 1994.

Chen, D., Fults, K. and Murphy M. The Primary Results for the First TxMLS Test Pad. *Paper Presented at the 76th Annual Meeting of the Transportation Research Board,* Washington, D.C., January 1997.

Chen, J.J., Hossain, M and Gisi, A. *Effect of Edge Conditions on FWD Testing and Data Analysis* Paper prepared for the 79'' Annual Meeting of the Transportation Research Board, January 2000.

Huang, Y.H. *Pavement Analysis and Design.* Prentice Hall, Inc., 1993.

Kaldate, R.R. and Hossain, M. *Mechanistic Evaluation of Superpave Level-I Mixtures.* Final Report. EES Report No. 283, Kansas Department of Transportation, Topeka, Kansas, May 1998.

McGennis, R.B. et al. *Background of SUPERPAVE Asphalt Mixture Design and Analysis.* Final Report No. FHWA-SA-95-003, Federal Highway Administration, Washington, D.C., November 1994.

Metcalf, J.B. *Application of Full-Scale Accelerated Pavement Testing. NCHRP Synthesis of Highway Practice* ***235,*** Transportation Research Board, Washington, D.C., 1996.

OECD Scientific Expert Group. *OECD Full-Scale Pavement Test.* OECD, 1991

Ullidtz, P., Askegaard, V and Sjolin, F. *Normal Stresses in a Granular Material Under Falling Weight Deflectometer Loading.* In Transportation Research Record 1540, Transportation Research Board, Washington, D.C., 1996.

Ullidtz, P. *Deterioration Models for Managing Flexible Pavements.* Paper Offered for Presentation at the 78'' Annual Meeting of the Transportation Research Board, Washington, D.C., 1998.

Vijaynanth, B.K., Wu, **Z.,** Hossain, M. and Gisi, A. *Instrumentation of the Superpave Test Sections at the Kansas Accelerated Testing Laboratory.* Proceedings of the International Conference on Accelerated Pavement Testing, Reno, Nevada, October 1999.

Yoder, E.J. and Witczak, M.W. *Principles of pavement Design.* John Wiley & Sons, Inc., 1975.